Scientific Research Publishing

Open Journal of Composite Materials, 2025, 15(2), 95-108
https://www.scirp.org/journal/ojcm
ISSN Online: 2164-5655
ISSN Print: 2164-5612

Impact of Ni Substitution on the Structural, Optical and Electronic Behavior of La_2CrMnO_6 Double Perovskite for Energy Applications

Jitendra Kumar Verma[1], Charu Agarwal[1,2], Tabassum Bano[1], Sunil Kumawat[3], Anuradha[3], Summaiyya Saleem[1], Mahendra Kumar Gora[1], Arvind Kumar[1], Subhash Chandra[1], Sanjay Kumar[1*]

[1]Department of Physics, University of Rajasthan, Jaipur, Rajasthan, India
[2]S.R.K.P. Govt. P.G. College, Kishangarh, Ajmer, India
[3]Department of Physics, University College of Science, M.L. Sukhadia, Udaipur, Rajasthan, India
Email: *sanjay.jnu@gmail.com

How to cite this paper: Verma, J.K., Agarwal, C., Bano, T., Kumawat, S., Anuradha, Saleem, S., Gora, M.K., Kumar, A., Chandra, S., and Kumar, S. (2025) Impact of Ni Substitution on the Structural, Optical and Electronic Behavior of La_2CrMnO_6 Double Perovskite for Energy Applications. *Open Journal of Composite Materials*, **15**, 95-108.
https://doi.org/10.4236/ojcm.2025.152005

Received: January 8, 2025
Accepted: March 14, 2025
Published: March 17, 2025

Abstract

Poly-crystalline double perovskite $La_2Cr_{1-x}Ni_xMnO_6$ ($x = 0.00, 0.50, 1.00$) has been synthesized by solid state reaction (SSR) method. Structural properties of $La_2Cr_{1-x}Ni_xMnO_6$ have been investigated using X-ray diffraction (XRD). The XRD pattern confirmed the single-phase formation of the orthorhombic structure having *Pbnm* symmetry. The morphological analysis of the synthesized sample was conducted using Scanning Electron Microscopy (SEM). The average particle size, determined from SEM micrographs, is 2 μm ($x = 0.00$), 1.56 μm ($x = 0.50$), and 1.32 μm ($x = 1.00$), indicating a progressive decrease in particle size with increasing nickel doping. The optical characteristics of the samples have been examined using UV-visible spectroscopy. The band gap has been found to be decreased with Ni doping. The XPS analysis verifies the presence of all elements at their respective binding energies and shows the splitting of Cr and Ni ions, which is attributed to spin-orbit coupling. The tuning of the optical band gap and the reduction in particle size in Ni-substituted La_2CrMnO_6 emphasize its potential for advancing future technological and energy applications.

Keywords

Solid State Reaction, Band Gap, XPS, Valance State

1. Introduction

A perovskite is defined as any substance with the formula PQX_3. P and Q are

two cations with positive charges, often of significantly different—different sizes, whereas X is an anion, generally oxygen, which forms bonds with both cations. Generally, P atoms are bigger than the Q atoms. Perovskites, as one of the most prominent structural families, are found in a wide range of compounds exhibiting diverse properties, applications, and importance, including metal-insulator transitions, and superconductivity [1]-[3]. Oxide-based double perovskites typically have the chemical formula $P_2QQ'O_6$, where P represents an element from the alkali metal, rare earth, or lanthanide families. The Q and Q' are transition metals coordinated with oxygen, forming two distinct octahedral sublattices, PO_6 and PQ'_6. The $P_2QQ'O_6$ perovskite may exhibit two distinct structures: a monoclinic structure with a $P2_1/n$ space group in the ordered state, or an orthorhombic *Pbnm* structure in the disordered state [4]. Examples of double perovskites with the formula $P_2QQ'O_6$ includes Tb_2NiMnO_6, Pr_2CoMnO_6, Ho_2NiMnO_6, Nd_2CoMnO_6, Gd_2CoMnO_6, La_2CoMnO_6, La_2NiMnO_6, Lu_2NiMnO_6 and La_2CrMnO_6. These materials exhibit a wide range of properties, such as piezoelectricity, ferroelectricity, and nonlinear optical behavior [5]. The modulation of Q-site cations by controlling structure, composition, defects, and dopants enhances the structural, optical, and electrical properties of these materials. This makes them promising candidates for industrial-scale applications such as solid oxide fuel cells, lead-free solar cells [6] [7], photovoltaics [8], superconductors, spintronics, and magnetoelectric devices [9] [10]. La_2CoMnO_6 and La_2NiMnO_6 are among the most prominent double perovskites due to their ability to form Q-site-ordered structures in bulk, exhibiting ferromagnetic insulating properties [11]-[13]. In contrast, other La_2QMnO_6 compounds, such as those with Q = V and Fe, do not display Q-site ordering in bulk form [14]. The double perovskite La_2CrMnO_6 serves as a suitable model for exploring the role of rare earth elements at the P-site and transition metals at the Q-site. However, experimental findings on La_2CrMnO_6 often reveal discrepancies and conflicting interpretations. In particular, its magnetic and electronic properties show significant variations across different studies [15] [16]. The double perovskite La_2CrMnO_6 is composed of two single perovskites, $LaCrO_3$ and $LaMnO_3$, with Cr and Mn ions distributed over disordered sites. The La cations occupy the interstitial spaces between the CrO_6 and MnO_6 octahedra, which are connected at their vertices and exhibit positional modifications along the three crystallographic axes [15]. The literature suggests that the double perovskite La_2CrMnO_6 can crystallize in different structural forms, depending on the synthesis method employed. La_2CrMnO_6 synthesized using the solid-state reaction method exhibited an orthorhombic structure with the *Pbnm* space group [17] [18]. Similarly, La_2CrMnO_6 synthesized via the sol-gel method also displays an orthorhombic structure with the Pbnm space group, accompanied by an optical band gap of approximately ~1 eV, which closely aligns with theoretical predictions [19]. Additionally, mesoporous La_2CrMnO_6 double perovskite prepared using the hydrothermal method exhibits a monoclinic structure with the $P2_1/n$ space group [20]. The electronic characteristics of perovskite compounds are mostly influenced by Q-site cations. Dou-

ble perovskites are characterized by their remarkable ability to incorporate a wide range of elements, particularly transition metals with varying oxidation states at the two Q-sites. This compositional flexibility accounts for the diverse properties observed in these materials, including semiconducting, metallic, half-metallic, dielectric, ferroelectric, thermoelectric, and potentially superconducting behaviors [5]-[9]. Notably, compounds containing transition metals often display the most intriguing electronic properties. Ni-substituted double perovskites have been extensively investigated for their potential in developing advanced materials for clean energy conversion and storage applications [21]-[25]. Structural transformations have been reported in earlier studies on Ni doping at the Ti site of $La_2CoTi_{(1-x)}Ni_xO_6$. The compound crystallizes in a monoclinic structure ($P2_1/n$) for $x = 0$, transitions to an orthorhombic structure ($Pbnm$) for $x = 0.2$, and adopts a rhombohedral phase ($R\bar{3}c$) for $x = 0.6$ [26]. XPS analysis shows that a 20% increase in nickel concentration notably impacts the mixed oxidation states of Co ions, resulting in alterations to bond lengths and causing a structural distortion from monoclinic to orthorhombic symmetry [26]. Ni-doped $CsPbBr_3$ halide perovskite, synthesized through a simple and efficient method, demonstrates improved luminescence efficiency, rendering it highly suitable for direct integration into optoelectronic devices [27]. Doping Ni ions into $CsPbBr_3$ induces a structural phase transition from orthorhombic to cubic, accompanied by lattice contraction caused by the partial substitution of Pb^{2+} ions with smaller Ni^{2+} ions within the $[PbBr_6]^{4-}$ octahedra. This transition is also associated with a slight increase in the band gap [27].

In this study, we successfully synthesized Ni-substituted La_2CrMnO_6 powder via the solid-state reaction method, demonstrating structural stability. We investigate the impact of Ni doping at the Cr site on the structural, optical, and electronic properties of $La_2Cr_{1-x}Ni_xMnO_6$. This work paves the way for future research on Ni-substituted La_2CrMnO_6, targeting the development of advanced materials for clean energy and storage applications.

2. Materials and Methods

The polycrystalline samples of $La_2Cr_{1-x}Ni_xMnO_6$ compounds ($x = 0.00, 0.50, 1.00$) were synthesized via the conventional solid-state reaction method. The starting materials used in the synthesis included reagent-grade Cr_2O_3 (AR), MnO_2 (AR), La_2O_3 (AR), and Ni_2O_3 (AR). The Polycrystalline Ni-doped La_2CrMnO_6 series was synthesized by combining stoichiometric amounts of La_2O_3, MnO_2, Cr_2O_3, and Ni_2O_3 in ethanol, milling the resultant mixture for seven hours, and then drying it at 1100˚C. The powder mixtures were reground for 4 hours, and after an interim grinding, they were calcined at 1300˚C for 10 hours in an environment of pure oxygen. To investigate the structural, surface, optical, and electronic properties of Ni-doped La_2CrMnO_6, samples were synthesized and designated as follows: $La_2Cr_{1-x}Ni_xMnO_6$ ($x = 0.00$) as LCMO, $La_2Cr_{1-x}Ni_xMnO_6$ ($x = 0.50$) as LCMO-Ni50, and $La_2Cr_{1-x}Ni_xMnO_6$ ($x = 1.00$) as LNMO.

3. Characterization Techniques

The investigation focused on analyzing the structural, optical, and electronic characteristics of the synthesized materials. The developed $La_2Cr_{1-x}Ni_xMnO_6$ material's crystal arrangement and phase purity were ascertained with the powder X-ray diffraction (XRD) technique. The XRD analysis was performed using a fifth-generation Rigaku X-ray diffractometer (Model no. MiniFlex 600) with a Cu-Kα source (wavelength = 1.5406 Å). A continuous scan was carried out within the 20˚ to 80˚ range, with a step size of 0.02˚. To evaluate the surface morphology and elemental composition of the samples, SEM and EDS images were recorded using the Nova Nano FE-SEM 450 (FEI). The optical properties were assessed using Ultra Violet-Visible Spectrometry (UV-Vis). A diffuse reflectance spectrum was recorded using a Shimadzu UV-2600 UV-visible spectrophotometer, covering a wavelength range of 200 to 800 nm. Furthermore, converting the DRS UV-Vis spectra to a Kubelka-Munk function, $[T(R)h\nu]^{1/2}$ vs. $E(h\nu)$ represented the indirect permissible band gap [28]. X-ray Photoelectron Spectroscopy (XPS) analysis of the surface structural characteristics of $La_2Cr_{1-x}Ni_xMnO_6$ (x = 0.00, 0.50, 1.00) was performed using a Thermo Scientific Nexa G2 XPS system under ultrahigh vacuum conditions. The data calibration was performed using the random C *1s* peak with a binding energy of 284.6 eV.

4. Results and Discussion

4.1. Structural Characterization

Understanding the crystal structure of a material is essential for gaining insight into its physical properties. XRD spectra were recorded to determine the crystal structure and detect the presence of any impurity phases in the as-prepared samples. **Figures 1(a)-(c)** present the XRD results of Ni-substituted $La_2Cr_{1-x}Ni_xMnO_6$ (x = 0.00, 0.50, 1.00) double perovskites recorded at room temperature. All the diffraction peaks were indexed to the *Pbnm* space group (No. 62), and their exact match with previously reported patterns [15] [17] [19]. This indicates that the original structure of La_2CrMnO_6 remains intact and does not undergo any phase transformation or structural instability upon Ni doping. The crystallite size of Ni-substituted $La_2Cr_{1-x}Ni_xMnO_6$ (x = 0.00, 0.50, 1.00) double perovskites was calculated using Scherrer's equation [19], yielding values of 36 nm for LCMO, 25 nm for LCMO-Ni50, and 20 nm for LNMO. These results exhibit a decreasing trend with increasing Ni substitution at the Cr site.

Figures 1(d)-(f) present an enlarged view of the X-ray diffraction pattern in the range of 2θ = 46˚ - 47.5˚, showing a peak shift to higher angles with Ni substitution at the Cr-site, as observed in the XRD spectra of the LCMO-Ni50 sample. The peak shift suggests slight lattice shrinkage, likely due to the variation in the ionic radii of Ni and Cr, consistent with explanations and observations reported in other Ni-substituted compounds [21] [23] [24] [29] and similar findings in materials with a tetragonal tungsten bronze (TTB) structure type [30].

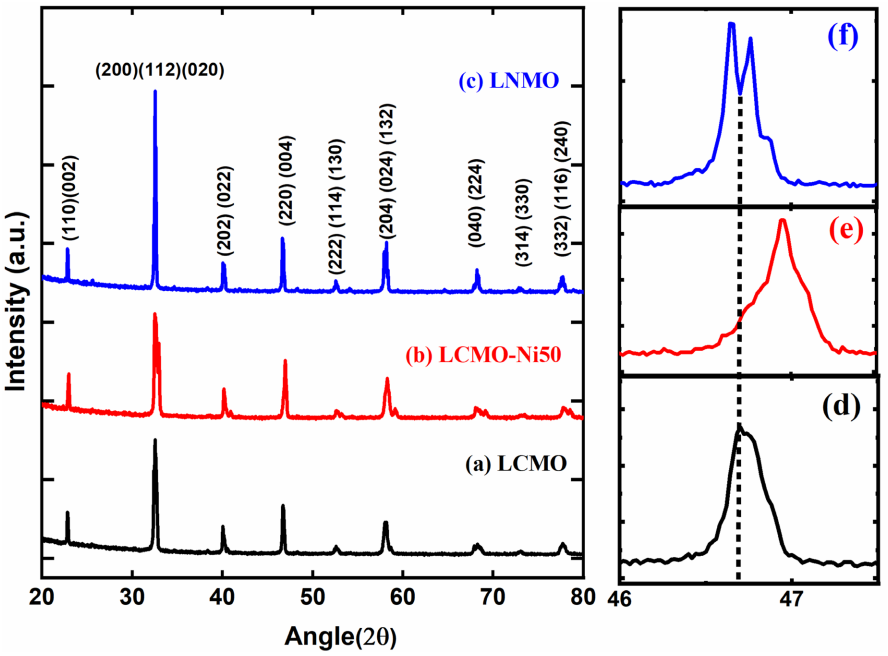

Figure 1. Room temperature X-ray diffraction patterns of $La_2Cr_{1-x}Ni_xMnO_6$ double perovskite material (a) LCMO ($x = 0$), (b) LCMO-Ni50 ($x = 50$), (c) LNMO ($x = 1$); (d)-(f) are the enlarged view of X-ray diffraction pattern in the range of $2\theta = 46^\circ$ - 47.5°.

Nickel (Ni) doping in oxide-based perovskite structures significantly impacts the crystal structure. These effects are influenced by factors such as the concentration of Ni dopants, the ionic radii of the dopant and host ions, and the oxidation state of Ni [23] [29] [31]. XRD patterns, along with the XPS survey (discussed in Section 4.4 below), confirm the presence of Cr, Ni, and Mn in their ionic states (ionic radius): Cr^{3+} (0.615 Å), Ni^{2+} (0.69 Å)/Ni^{3+} (0.60 Å), and Mn^{3+} (0.65 Å)/Mn^{4+} (0.53 Å), respectively, which aligns with those reported in previous studies [23] [24] [29] [31]. Ni^{2+} ions, being larger than Ni^{3+} ions, cause greater lattice expansion or distortion, while Ni^{3+} ions, with a smaller radius, contribute to lattice contraction, balancing structural changes in Ni-substituted $La_2Cr_{1-x}Ni_xMnO_6$ samples [29]. The substitution of Ni^{2+} at the Cr^{3+} site results in changes to particle size and grain size (discussed in Section 4.2), which could potentially enable tuning of the optical and electrical properties in the La_2CrMnO_6 system, similar to modifications observed in compounds with a tetragonal tungsten bronze (TTB) structure type [32] [33].

4.2. Surface Analysis

Field Emission Scanning Electron Microscopy (FESEM), shown in **Figures 2(a)-(c)**, and Energy-Dispersive X-ray Analysis (EDX), shown in **Figures 3(a)-(c)**, were conducted to examine the surface morphology and elemental composition of the as-synthesized samples. As shown in **Figures 2(a)-(c)**, the SEM images reveal a lack of discernible grain boundary formation, with most grains exhibiting independent growth, similar to the behavior observed in Bi-substituted La_2CoMnO_6

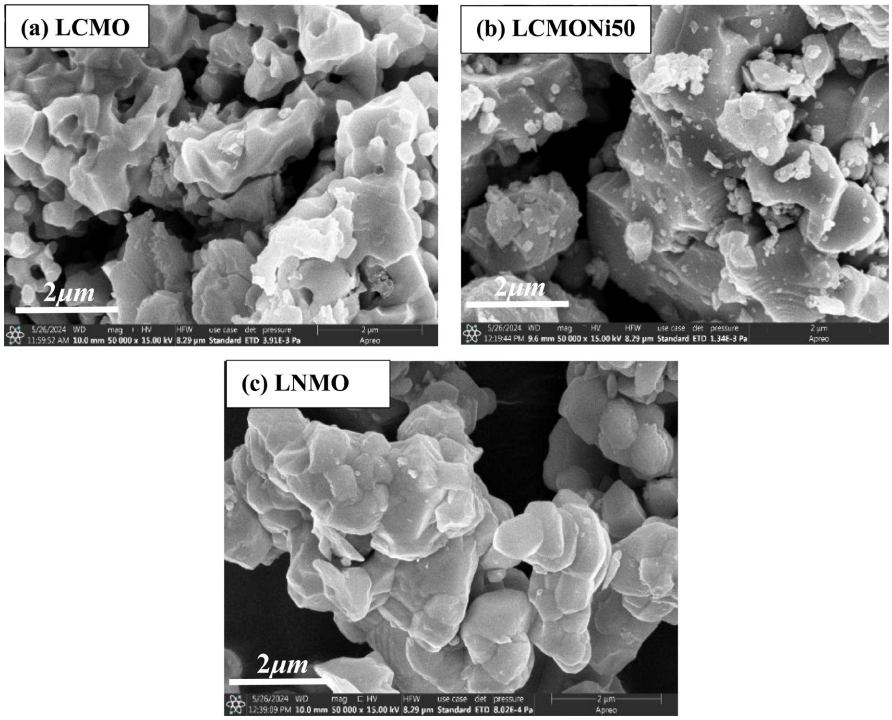

Figure 2. FESEM images of Ni-substituted $La_2Cr_{1-x}Ni_xMnO_6$ (x = 0.00, 0.50, 1.00) double perovskite: (a) LCMO, (b) LCMO-Ni50, and (c) LNMO.

compounds [28]. **Figures 3(a)-(c)** present the EDX analysis of the structural and chemical properties of LCMO, LCMO-Ni50, and LNMO samples, corresponding to the SEM images shown previously. The EDX spectra indicate that all samples (LCMO, LCMO-Ni50, and LNMO) have retained their key elements, particularly Ni, as evidenced by the corresponding energy peaks and their concentration levels [18] [19] [34]. The EDX spectra also confirm the absence of any foreign elements, thereby justifying the phase purity in the LCMO, LCMO-Ni50, and LNMO samples. Grain size, average particle size, and area were determined using ImageJ Software, with the corresponding data provided in **Table 1**. The average particle size, as determined from the SEM micrographs, is 2 μm for LCMO, 1.56 μm for LCMO-Ni50, and 1.32 μm for LNMO, indicating a gradual decrease in particle size with increasing nickel doping. The mean particle size of the materials, analyzed using SEM micrographs, shows a good correlation with the XRD patterns. The average grain size reported for LCMO, LCMO-Ni50, and LNMO is in the

Table 1. The average grain size, particle size and band gap of Ni-substituted $La_2Cr_{1-x}Ni_xMnO_6$ (x = 0.00, 0.50, 1.00) double perovskite.

Sample	Area (μm²)	Average Particle Size (μm)	Grain Size (μm)	Band gap (eV)
LCMO	182.33	2	131.718	1.12
LCMO-Ni50	182.33	1.56	119.279	0.98
LNMO	182.33	1.32	112.488	0.95

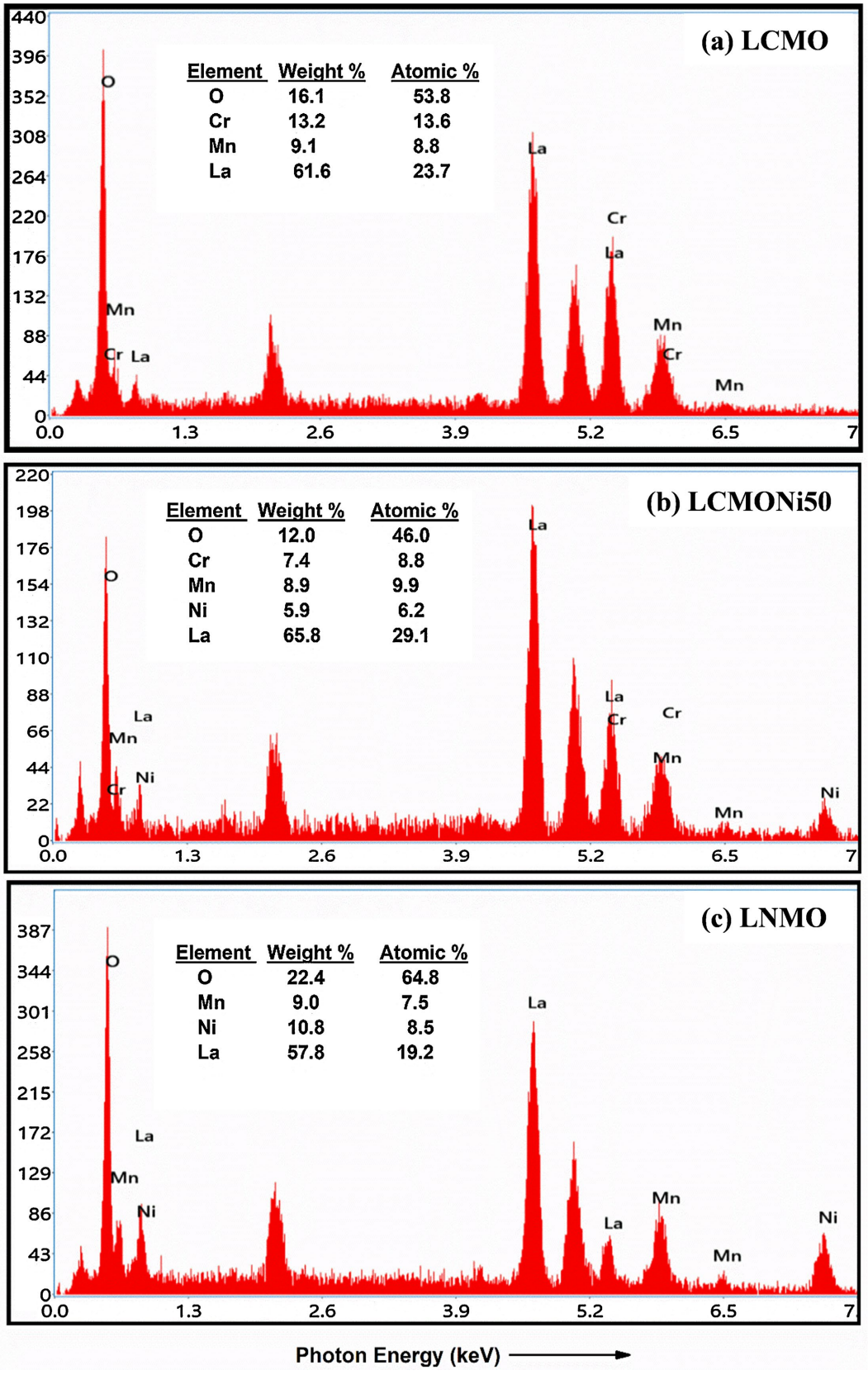

Figure 3. EDAX spectra of Ni-substituted $La_2Cr_{1-x}Ni_xMnO_6$ (x = 0.00, 0.50, 1.00) double perovskite: (a) LCMO, (b) LCMO-Ni50, and (c) LNMO.

micrometer range, while the crystallite size is in the nanometer range, confirming the polycrystalline nature of all samples with relatively large grain sizes, consistent with observations in Ni-substituted Ca_2FeNbO_6 double perovskite compounds [35].

As shown in Table 1, the grain size progressively decreases with increasing Ni concentration, which is consistent with findings reported in previous studies [28]. The distribution of chemical components in $La_2Cr_{1-x}Ni_xMnO_6$ (x = 0.00, 0.50, 1.00) confirms that it follows the intended stoichiometric ratio, as expected. The intriguing SEM analysis data, including the reduction in grain size and average particle size with Ni substitution at the Cr site, highlights the potential for further research to enhance the electrical properties of Ni-substituted La_2CrMnO_6 double perovskite.

4.3. Optical Properties

The optical bandgap properties were meticulously studied to obtain a deeper understanding of the electronic band structure in Ni-substituted La_2CrMnO_6 double perovskites. The diffuse reflectance UV-Vis spectra of the samples were recorded over the wavelength range of 200 - 800 nm, as illustrated in Figure 4. Figures 4(a)-(c)

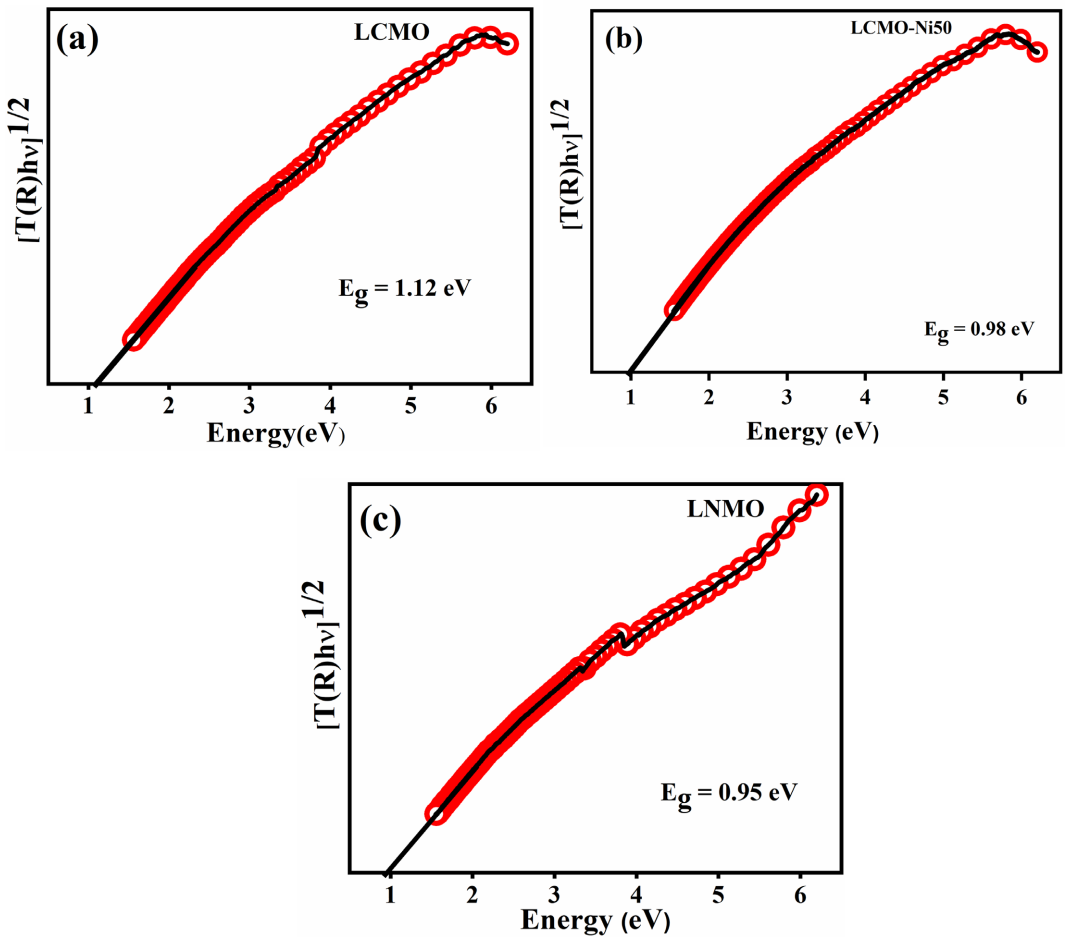

Figure 4. Ni-substituted $La_2Cr_{1-x}Ni_xMnO_6$ (x = 0.00, 0.50, 1.00) double perovskite: (a) LCMO, (b) LCMO-Ni50, and (c) LNMO.

depicts the relationship between $[T(R)h\nu]^{1/2}$ and $E(h\nu)$ for an indirect band gap, determined by converting the DRS UV-Vis spectra into the Kubelka-Munk function, following the methodology established in prior studies [28].

The sharp edge of each curve was extrapolated to intersect the energy axis. The intercept at this edge provides the energy band gap values, which were calculated as 1.12 eV, 0.98 eV, and 0.95 eV for LCMO, LCMO-Ni50, and LNMO samples. These findings are summarized in Table 1. As the quantity of Ni doping increases, all the samples show a progressive drop in bandgap values. The reduction in the band gap can be attributed to the substitution of Ni^{2+} ions at Cr^{3+} ions, which may introduce additional electronic states near the Fermi level, thereby narrowing the band gap [35]-[38]. Furthermore, the difference in ionic radii between Ni^{2+} (0.69 Å) and Cr^{3+} (0.615 Å), along with the reduction in crystallite size, may induce structural distortions, as indicated by the peak shifts in the XRD patterns, thereby affecting the electronic band structure [35] [38]. Ni substitution at the Cr site in La_2CrMnO_6 strongly correlates structural distortions and crystallite size reduction with optical properties. This makes these materials promising for advanced technologies requiring precise band gap engineering.

4.4. Electronic Properties

The magnetic exchange interactions of most compounds are very responsive to variations in their oxidation states. An extensive examination of the oxidation states of Cr and Ni ions in the $La_2Cr_{1-x}Ni_xMnO_6$ series using X-ray photoelectron spectroscopy is essential for a thorough comprehension of its magnetic characteristics. To examine the chemical valence states of La, Cr, Ni, and Mn in $La_2Cr_{1-x}Ni_xMnO_6$ for (x = 0.00, 0.50, 1.00), XPS investigation was conducted at room temperature. Figure 5 illustrates the XPS survey spectra of the synthesized samples, showcasing the photoelectron lines corresponding to chromium, oxygen, lanthanum, manganese, and nickel. The observed peak positions are consistent

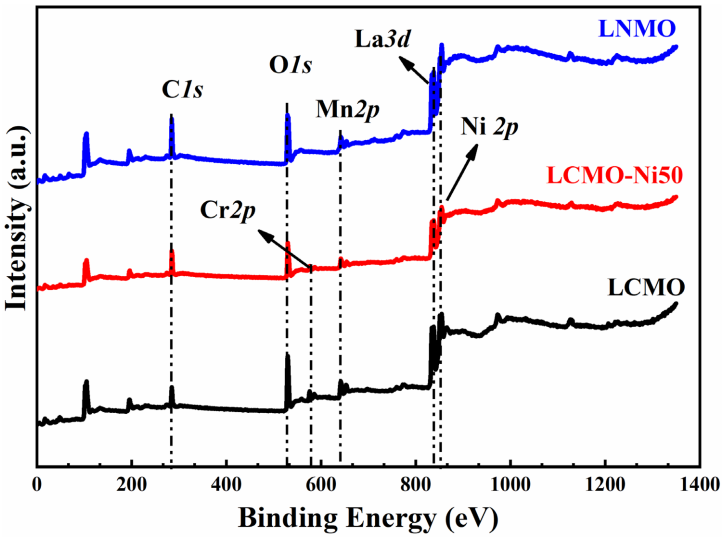

Figure 5. XPS Survey spectra of LCMO, LCMO-Ni50 and LNMO samples.

with those reported in previous studies [20] [34] [39]. Figure 6 presents the XPS spectra for the O 1s and C 1s core-level regions. The C 1*s* line with a binding energy of 284.6 eV is apparent in the spectrum, presumably due to the presence of this element on the powder's surface, as shown in Figure 6(a). The core level XPS spectra of O 1*s*, Cr 2*p*, Mn 2*p* and Ni 2*p* are obtained to elucidate their chemical valences. The asymmetric profile of the O 1s XPS high-resolution spectra for all synthesized samples, shown in Figure 6(b), reveals a distinct shoulder on the high binding energy side, with a prominent peak around ~529 eV, which is

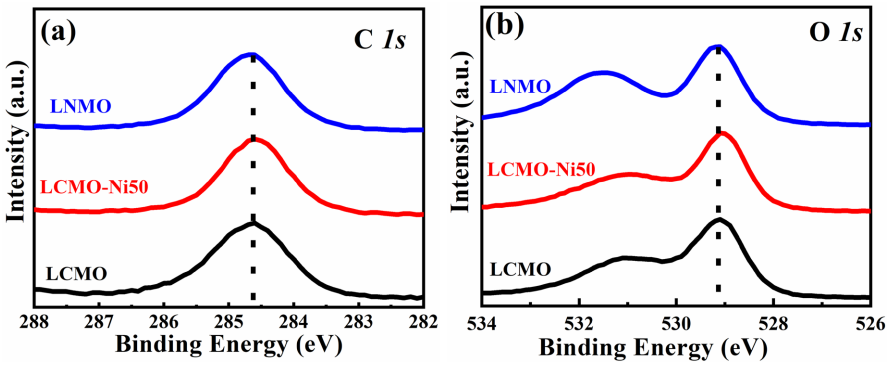

Figure 6. XPS survey spectra of LCMO, LCMO-Ni50 and LNMO samples, showing (a) C 1*s* and (b) O 1*s* core-level regions.

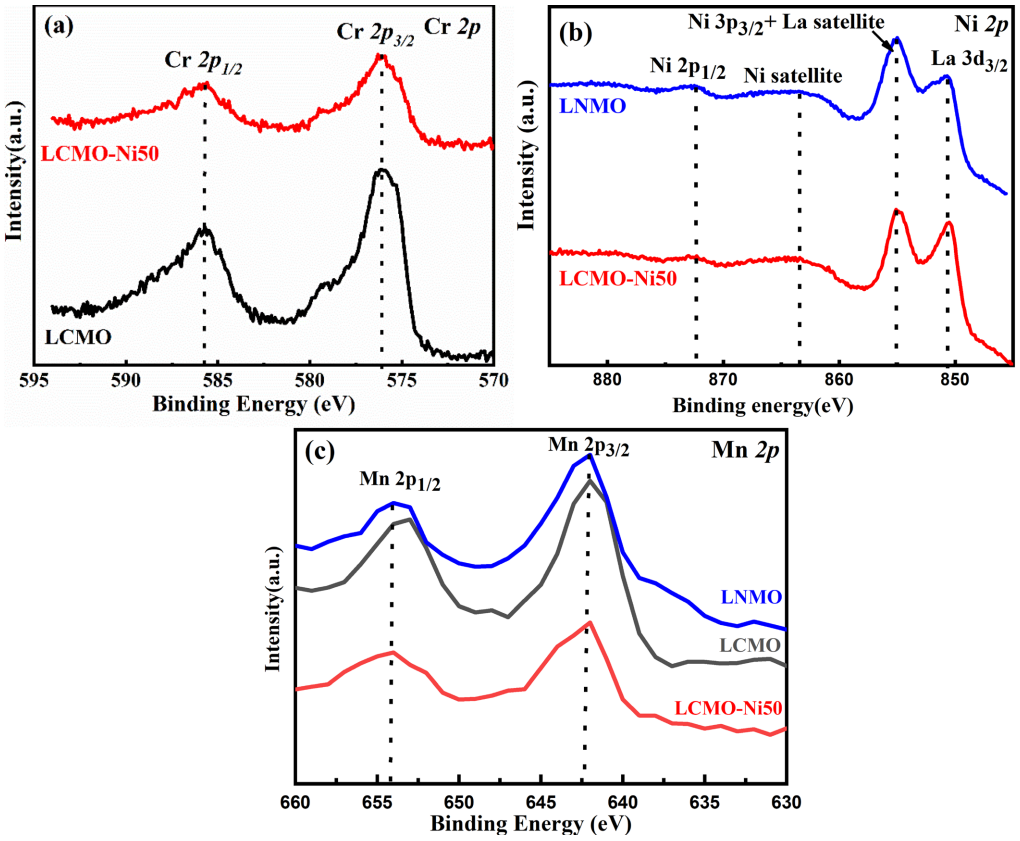

Figure 7. XPS survey spectra of LCMO, LCMO-Ni50 and LNMO samples, showing (a) Cr 2*p*, (b) Ni 2*p*, and (c) Mn 2*p* core-level regions.

consistent with previous reports [18] [20] [31] [34]. The chemical states of Ni, Cr, and Mn in the LCMO, LCMO-Ni50, and LNMO samples were investigated through XPS analysis, as depicted in **Figure 7**. The XPS spectrum of chromium shows a clear splitting of the Cr 2*p* peak into two spectral lines, $2p_{3/2}$ and $2p_{1/2}$, at approximately ~575 eV and ~585 eV for both LCMO and LCMO-Ni50, as shown in **Figure 7(a)** [1] [17]. The splitting of the Cr 2p core-level spectrum at ~575 eV and ~585 eV is attributed to spin-orbit coupling and corresponds to the Cr^{3+} ionic state, as validated by previously reported data [18] [39] [40].

The XPS spectrum of nickel for both LCMO-Ni50 and LNMO, shown in **Figure 7(b)**, reveals a mixed valence state of Ni^{2+} and Ni^{3+}, with the binding energy peak positions consistent with previously reported data [20] [31] [34]. The satellite features of Ni $2p_{3/2}$ and La $3d_{3/2}$ overlap with one another, as observed in previous studies [31] [39]. **Figure 7(c)** illustrates the XPS survey of the Mn 2*p* core-level peaks, revealing two primary features: Mn $2p_{3/2}$ peak at ~642 eV and Mn $2p_{1/2}$ peak at ~654 eV. These peaks arise due to spin-orbit coupling. The observed peak positions of Mn $2p_{3/2}$ and Mn $2p_{1/2}$ align precisely with values reported in the literature, confirming the presence of Mn in mixed oxidation states, Mn^{3+} and Mn^{4+} [17] [18] [20] [31] [34]. The XPS results confirm the presence of mixed valence states for both Ni and Mn ions in Ni-substituted La_2CrMnO_6 double perovskites.

5. Conclusion

In summary, Ni-substituted $La_2Cr_{1-x}Ni_xMnO_6$ ($x = 0.00, 0.50, 1.00$) double perovskites were synthesized using the conventional solid-state reaction method. The structural, optical, morphological, and electronic properties of these materials have been thoroughly investigated. The XRD patterns confirm that all samples crystallized in the *Pbnm* space group, exhibiting an orthorhombic structure without any impurity peaks, ensuring phase purity. The crystallite size decreases with increasing Ni content at the Cr site. The observed peak shifts in the XRD patterns further confirm the distortion of the $(Cr/Mn/Ni)O_6$ octahedra. Optical investigation, combined with morphological analysis, reveals a decreasing trend in average particle size, grain size, and optical band gap with Ni substitution at the Cr site, suggesting that Ni-substituted La_2CrMnO_6 could be a promising candidate for future energy conversion technologies. The XPS survey indicates the presence of mixed ionic states for Ni (Ni^{2+}/Ni^{3+}) and Mn (Mn^{3+}/Mn^{4+}). These findings pave the way for future studies aimed at enhancing the electrical and electrochemical properties of these materials, making them promising candidates for photovoltaic technology.

Acknowledgements

The authors express their sincere gratitude to Dr. Monika Rani, Mohanlal Sukhadia University, Udaipur, Rajasthan, for performing the XRD measurements, the Department of Physics, University of Rajasthan, Jaipur, for supporting the XPS measurements, and the Central Analytical Facilities, Manipal University Jaipur,

for their assistance with the optical studies.

Conflicts of Interest

The authors declare no conflicts of interest regarding the publication of this paper.

References

[1] Artini, C. (2017) Crystal Chemistry, Stability and Properties of Interlanthanide Perovskites: A Review. *Journal of the European Ceramic Society*, **37**, 427-440. https://doi.org/10.1016/j.jeurceramsoc.2016.08.041

[2] Imada, M., Fujimori, A. and Tokura, Y. (1998) Metal-Insulator Transitions. *Reviews of Modern Physics*, **70**, 1039-1263. https://doi.org/10.1103/revmodphys.70.1039

[3] Monthoux, P., Pines, D. and Lonzarich, G.G. (2007) Superconductivity without Phonons. *Nature*, **450**, 1177-1183. https://doi.org/10.1038/nature06480

[4] Zhou, H.Y. and Chen, X.M. (2017) Structural Distortions, Orbital Ordering and Physical Properties of Double Perovskite R_2CoMnO_6 Calculated by First-Principles. *Journal of Physics*: *Condensed Matter*, **29**, Article ID: 145701. https://doi.org/10.1088/1361-648x/aa5e3e

[5] Newnham, R.E. and Ruschau, G.R. (1991) Smart Electroceramics. *Journal of the American Ceramic Society*, **74**, 463-480. https://doi.org/10.1111/j.1151-2916.1991.tb04047.x

[6] Lan, C., Zhao, S., Xu, T., Ma, J., Hayase, S. and Ma, T. (2016) Investigation on Structures, Band Gaps, and Electronic Structures of Lead Free La_2NiMnO_6 Double Perovskite Materials for Potential Application of Solar Cell. *Journal of Alloys and Compounds*, **655**, 208-214. https://doi.org/10.1016/j.jallcom.2015.09.187

[7] Aarif Ul Islam, S. and Ikram, M. (2019) Structural Stability Improvement, Williamson Hall Analysis and Band-Gap Tailoring through A-Site Sr Doping in Rare Earth Based Double Perovskite La_2NiMnO_6. *Rare Metals*, **38**, 805-813. https://doi.org/10.1007/s12598-019-01207-4

[8] Sariful Sheikh, M., Ghosh, D., Dutta, A., Bhattacharyya, S. and Sinha, T.P. (2017) Lead Free Double Perovskite Oxides Ln_2NiMnO_6 (Ln = La, Eu, Dy, Lu), a New Promising Material for Photovoltaic Application. *Materials Science and Engineering*: *B*, **226**, 10-17. https://doi.org/10.1016/j.mseb.2017.08.027

[9] Jose, R., Konopka, J., Yang, X., Konopka, A., Ishikawa, M. and Koshy, J. (2004) Crystal Structure and Dielectric Properties of a New Complex Perovskite Oxide Ba_2LaSbO_6. *Applied Physics A*, **79**, 2041-2047. https://doi.org/10.1007/s00339-004-2672-4

[10] Mandal, P.R., Sahoo, R.C. and Nath, T.K. (2014) A Comparative Study of Structural, Magnetic, Dielectric Behaviors and Impedance Spectroscopy for Bulk and Nanometric Double Perovskite Sm_2CoMnO_6. *Materials Research Express*, **1**, Article ID: 046108. https://doi.org/10.1088/2053-1591/1/4/046108

[11] Blasse, G. (1965) Ferromagnetic Interactions in Non-Metallic Perovskites. *Journal of Physics and Chemistry of Solids*, **26**, 1969-1971. https://doi.org/10.1016/0022-3697(65)90231-3

[12] Dass, R.I. and Goodenough, J.B. (2003) Multiple Magnetic Phases of $La_2CoMnO_{6-\delta}$ ($0 < \sim\delta < \sim 0.05$). *Physical Review B*, **67**, Article ID: 014401. https://doi.org/10.1103/physrevb.67.014401

[13] Dass, R.I., Yan, J. and Goodenough, J.B. (2003) Oxygen Stoichiometry, Ferromagnetism, and Transport Properties of $La_{2-x}NiMnO_{6+\delta}$. *Physical Review B*, **68**, Article ID: 064415. https://doi.org/10.1103/physrevb.68.064415

[14] Androulakis, J., Katsarakis, N. and Giapintzakis, J. (2002) Realization of La_2MnVO_6: Search for Half-Metallic Antiferromagnetism? *Solid State Communications*, **124**, 77-81. https://doi.org/10.1016/s0038-1098(02)00490-8

[15] Palakkal, J.P., Raj Sankar, C. and Varma, M.R. (2017) Multiple Magnetic Transitions, Griffiths-Like Phase, and Magnetoresistance in La_2CrMnO_6. *Journal of Applied Physics*, **122**, Article ID: 073907. https://doi.org/10.1063/1.4999031

[16] Singh, D. and Mahajan, A. (2015) Effect of A-Site Cation Size on the Structural, Magnetic, and Electrical Properties of $La_{1-x}Nd_xMn_{0.5}Cr_{0.5}O_3$ Perovskites. *Journal of Alloys and Compounds*, **644**, 172-179. https://doi.org/10.1016/j.jallcom.2015.04.180

[17] Yang, D., Zhao, P., Huang, S., Yang, T. and Huo, D. (2019) Ferrimagnetism, Resistivity, and Magnetic Exchange Interactions in Double Perovskite La_2CrMnO_6. *Results in Physics*, **12**, 344-348. https://doi.org/10.1016/j.rinp.2018.11.090

[18] Mahato, D.K., Molak, A., Szeremeta, A.Z., Gruszka, I., Zajdel, P., Pilch, M., *et al.* (2018) Determination of Polaronic Conductivity in Disordered Double Perovskite La_2CrMnO_6. *Journal of Electroceramics*, **42**, 136-146. https://doi.org/10.1007/s10832-018-0164-8

[19] Khan, J.A. and Ahmad, J. (2019) Double Perovskite La_2CrMnO_6: Synthesis, Optical and Transport Properties. *Materials Research Express*, **6**, Article ID: 115906. https://doi.org/10.1088/2053-1591/ab4728

[20] Singh, A., Vasishth, A. and Kumar, A. (2023) Hydrothermal Synthesis and Electrochemical Performance of Mesoporous La_2CrMnO_6 Double Perovskite for Energy Storage Applications. *Physica Status Solidi* (*a*), **220**, Article ID: 2300198. https://doi.org/10.1002/pssa.202300198

[21] Rahumi, O., Rath, M.K., Meshi, L., Rozenblium, I. and Borodianskiy, K. (2024) Ni-doped SFM Double-Perovskite Electrocatalyst for High-Performance Symmetrical Direct-Ammonia-Fed Solid Oxide Fuel Cells. *ACS Applied Materials & Interfaces*, **16**, 53652-53664. https://doi.org/10.1021/acsami.4c07968

[22] Chen, L., Yuan, C., Xue, J. and Wang, J. (2005) B-Site Ordering and Magnetic Behaviours in Ni-Doped Double Perovskite Sr_2FeMoO_6. *Journal of Physics D*: *Applied Physics*, **38**, 4003-4008. https://doi.org/10.1088/0022-3727/38/22/001

[23] Dai, N., Feng, J., Wang, Z., Jiang, T., Sun, W., Qiao, J., *et al.* (2013) Synthesis and Characterization of B-Site Ni-Doped Perovskites $Sr_2Fe_{1.5-x}Ni_xMo_{0.5}O_{6-\delta}$ (x = 0, 0.05, 0.1, 0.2, 0.4) as Cathodes for SOFCs. *Journal of Materials Chemistry A*, **1**, 14147. https://doi.org/10.1039/c3ta13607h

[24] Meng, X., Wang, Y., Zhao, Y., Zhang, T., Yu, N., Chen, X., *et al.* (2020) *In-Situ* Exsolution of Nanoparticles from Ni Substituted $Sr_2Fe_{1.5}Mo_{0.5}O_6$ Perovskite Oxides with Different Ni Doping Contents. *Electrochimica Acta*, **348**, Article ID: 136351. https://doi.org/10.1016/j.electacta.2020.136351

[25] Harbi, A., Moutaabbid, H., Li, Y., Renero-Lecuna, C., Fialin, M., Le Godec, Y., *et al.* (2019) The Effect of Cation Disorder on Magnetic Properties of New Double Perovskites $La_2Ni_xCo_{1-x}MnO_6$ (x = 0.2–0.8). *Journal of Alloys and Compounds*, **778**, 105-114. https://doi.org/10.1016/j.jallcom.2018.10.360

[26] Solanki, N., Choudhary, R.J. and Kaurav, N. (2023) Qualitative Study of Structural Phase Transition in Nickel Doped $La_2CoTi_{(1-x)}Ni_xO_6$ Double Perovskite. *Journal of Alloys and Compounds*, **943**, Article ID: 169126. https://doi.org/10.1016/j.jallcom.2023.169126

[27] Chen, T., Liu, R., Tang, S., Li, X., Ye, S., Duan, X., *et al.* (2021) Ni^{2+} Doping Induced Structural Phase Transition and Photoluminescence Enhancement of $CsPbBr_3$. *AIP Advances*, **11**, Article ID: 115008. https://doi.org/10.1063/5.0067153

[28] Bajpai, N., Saleem, M. and Mishra, A. (2020) Effect of Bismuth (Bi^{3+}) Substitution on Structural, Optical, Dielectric and Magnetic Nature of La_2CoMnO_6 Double Perovskite. *Journal of Materials Science*: *Materials in Electronics*, **32**, 12890-12902. https://doi.org/10.1007/s10854-020-04348-w

[29] Qahtan, A.A.A., Husain, S. and Khan, W. (2021) The Effect of Ni Doping on the Structural, Optical and Dielectric Properties of Nanocrystalline $YbCrO_3$. *Journal of Physics and Chemistry of Solids*, **159**, Article ID: 110280. https://doi.org/10.1016/j.jpcs.2021.110280

[30] Es-soufi, H., Sayyed, M.I., Almuqrin, A.H., Rajesh, R., Lima, A.R.F., Bih, H., *et al.* (2023) Crystallographic, Structural, and Electrical Properties of W^{6+} Substituted with Mo^{6+} in Crystalline Phases Such as TTB Structure. *Crystals*, **13**, Article No. 483. https://doi.org/10.3390/cryst13030483

[31] Nasir, M., Khan, M., Rini, E.G., Agbo, S.A. and Sen, S. (2021) Exploring the Role of Fe Substitution on Electronic, Structural, and Magnetic Properties of La_2NiMnO_6 Double Perovskites. *Applied Physics A*, **127**, Article No. 208. https://doi.org/10.1007/s00339-021-04361-8

[32] Es-Soufi, H., Lahmar, A., Rajesh, R., Bih, H. and Bih, L. (2024) Exploration of the Crystal Structure and Impedance Spectroscopy Characteristics in $Ba_{0.54}Na_{0.46}Nb_{1.29}W_{0.37}O_5$ Crystalline Phase. *Nexus of Future Materials*, **1**, 20-25. https://doi.org/10.70128/584045

[33] Es-soufi, H., Lahmar, A., Rajesh, R., Sayyed, M.I., Bih, H. and Bih, L. (2024) Crystallographic, Structural, and Electrical Characteristics of a New Molybdate Crystalline Phase within the $NaNbO_3$-$BaNb_2O_6$-MoO_3 System. *Optical and Quantum Electronics*, **56**, Article No. 1337. https://doi.org/10.1007/s11082-024-07116-w

[34] Yi, K., Tang, Q., Wu, Z. and Zhu, X. (2022) Unraveling the Structural, Dielectric, Magnetic, and Optical Characteristics of Nanostructured La_2NiMnO_6 Double Perovskites. *Nanomaterials*, **12**, Article No. 979. https://doi.org/10.3390/nano12060979

[35] Mohanty, S. and Behera, S. (2023) Multifunctional Properties of Transition Metal Based Double Perovskite Ceramics. *Chemical Physics Impact*, **7**, Article ID: 100259. https://doi.org/10.1016/j.chphi.2023.100259

[36] Saleem, M., Tiwari, S., Soni, M., Bajpai, N. and Mishra, A. (2020) Structural, Optical and Other Spectral Studies of Transition Metal Ti^{4+}-Doped Zn-Cd Oxide Nanomaterials. *International Journal of Modern Physics B*, **34**, Article ID: 2050033. https://doi.org/10.1142/s0217979220500332

[37] Zhou, W., Deng, H., Yu, L., Yang, P. and Chu, J. (2015) Optical Band-Gap Narrowing in Perovskite Ferroelectric ABO_3 Ceramics (A = Pb, Ba; B = Ti) by Ion Substitution Technique. *Ceramics International*, **41**, 13389-13392. https://doi.org/10.1016/j.ceramint.2015.07.127

[38] Mohanty, S., Satapathy, S., Nayak, M., Rai, S., Singh, R. and Behera, S. (2024) Effect of Low Ni-Substitution on Optical, Dielectric and Magnetic Properties of Double Perovskite Mg_2FeNbO_6. *Inorganic Chemistry Communications*, **165**, Article ID: 112513. https://doi.org/10.1016/j.inoche.2024.112513

[39] Biesinger, M.C., Payne, B.P., Grosvenor, A.P., Lau, L.W.M., Gerson, A.R. and Smart, R.S.C. (2011) Resolving Surface Chemical States in XPS Analysis of First Row Transition Metals, Oxides and Hydroxides: Cr, Mn, Fe, Co and Ni. *Applied Surface Science*, **257**, 2717-2730. https://doi.org/10.1016/j.apsusc.2010.10.051

[40] Uekawa, N. and Kaneko, K. (1996) Dopant Reduction in P-Type Oxide Films upon Oxygen Absorption. *The Journal of Physical Chemistry*, **100**, 4193-4198. https://doi.org/10.1021/jp952784m